Biochimica et Biophysica Acta 1864 (2017) 113–124

Contents lists available at ScienceDirect

Biochimica et Biophysica Acta

journal homepage: www.elsevier.com/locate/bbamcr

RIP3 antagonizes a TSC2-mediated pro-survival pathway in glioblastoma cell death

Gregory Fettweis [a], Emmanuel Di Valentin [b], Laurent L'homme [a], Cédric Lassence [a], Franck Dequiedt [c], Marianne Fillet [d], Isabelle Coupienne [a], Jacques Piette [a,*]

[a] Laboratory of Virology and Immunology, GIGA-I³, University of Liège, Liège, Belgium
[b] GIGA-Viral Vector Platform, University of Liège, Liège, Belgium
[c] Laboratory of Protein Signaling and Interactions, GIGA-Molecular Biology of Diseases, University of Liège, Liège, Belgium
[d] Laboratory for the Analysis of Medicines (LAM), Department of Pharmaceutical Sciences, CIRM, University of Liège, Liège, Belgium

ARTICLE INFO

Article history:
Received 1 July 2016
Received in revised form 29 September 2016
Accepted 25 October 2016
Available online 27 October 2016

Keywords:
Photodynamic therapy
Glioblastoma
Autophagy regulation
Programmed necrosis
MAP kinases

ABSTRACT

Glioblastomas are the deadliest type of brain cancer and are frequently associated with poor prognosis and a high degree of recurrence despite removal by surgical resection and treatment by chemo- and radio-therapy. Photodynamic therapy (PDT) is a treatment well known to induce mainly necrotic and apoptotic cell death in solid tumors. 5-Aminolevulinic acid (5-ALA)-based PDT was recently shown to sensitize human glioblastoma cells (LN-18) to a RIP3 (Receptor Interacting Protein 3)-dependent cell death which is counter-acted by activation of autophagy. These promising results led us to investigate the pathways involved in cell death and survival mechanisms occurring in glioblastoma following PDT. In the present study, we describe a new TSC2 (Tuberous Sclerosis 2)-dependent survival pathway implicating MK2 (MAPKAPK2) kinase and 14-3-3 proteins which conducts to the activation of a pro-survival autophagy. Moreover, we characterized a new RIP3/TSC2 complex where RIP3 is suggested to promote cell death by targeting TSC2-dependent survival pathway. These results highlight (i) a new role of TSC2 to protect glioblastoma against PDT-induced cell death and (ii) TSC2 and 14-3-3 as new RIP3 partners.

1. Introduction

Glioblastomas are among the most frequent and deadliest human brain tumors [1]. The current therapeutic strategy involves surgical resection combined with chemo- and radio-therapy [2–4]. Despite extensive research, efficient long-term treatments remain elusive and glioblastomas are associated with a high degree of recurrence and a median of survival of 14 months. Several genetic alterations have been associated with glioblastoma, which culminate in deregulation of major signaling pathways such as those including EGFR, p53 and overactivation of the NF-κB and AKT/mTOR axis [5,6].

Photodynamic therapy (PDT) is a promising treatment against solid tumors, especially glioblastoma for which this treatment is considered now as a treatment of choice among a few neurosurgical therapeutic opportunities [7]. This therapy relies on a photosensitizer, which upon illumination by visible light of specific wavelength, produces a burst of ROS (Reactive Oxygen Species) that can lead to cell death. In this study we used the 5-aminolevulinic acid (5-ALA) prodrug approach which is known to lead to the accumulation of protoporphyrin IX (PPIX) in mitochondria [8]. Indeed, in the heme cycle, 5-ALA is metabolized in photosensitive PPIX which selectively accumulates in tumor cells due to their low ferrochelatase levels [9]. Interestingly, this high selectivity for tumor cells is frequently used for fluorescence guided resection by neuro-surgeons, and notably for glioblastomas [10]. In addition, it was shown that PDT can successfully expand the survival of patients suffering from non-resectable glioblastoma tumors [11–13].

Previously, we showed that two antagonistic signaling pathways are involved in PDT-induced glioblastoma cell death. First, 5-ALA-PDT induces in glioblastoma a strong pro-survival autophagy *via* a still incompletely described mechanism [14]. This autophagy process is directly regulated by TSC2 (Tuberous Sclerosis 2), a protein known to be regulated by phosphorylation [15], ubiquitination [16] and acetylation [17], which associates with TSC1. The TSC2-TSC1 complex down-regulates the mTOR complex activity, which represses the autophagy pathway and promotes survival and proliferation [18]. As we have previously shown, activation of mTOR downstream effectors was reduced after PDT, suggesting a down-regulation of the mTOR complex activity and a subsequent possible rise of the autophagic flux [14]. On the other hand, PDT is known to induce both necrosis and apoptosis in

Abbreviations: 5-ALA, 5-aminolevulinic acid; MK2, MAP Kinase-Activated Protein kinase 2; p38, Mitogen-Activated Protein kinase p38; PDT, Photodynamic Therapy; RIP, Receptor Interacting Protein; TSC, Tuberous Sclerosis; YWHA, Tyrosine 3-Monooxygenase/Tryptophan 5-Monooxygenase Activation Protein, 14-3-3 proteins.

* Corresponding author at: Laboratory of Virology and Immunology, GIGA-R B34, University of Liege, 1 Avenue de l'Hôpital, Liège 4000, Belgium.
E-mail address: jpiette@ulg.ac.be (J. Piette).

http://dx.doi.org/10.1016/j.bbamcr.2016.10.014
0167-4889/

glioblastoma [19,20]. Recently, Receptor Interacting Protein kinase 3 (RIP3), a key protein of the programmed necrosis pathway (necroptosis) was demonstrated to be involved in PDT-induced glioblastoma cell death induced by PDT [21–23] and other cell death inducers [24–26]. The current model of necroptosis relies on the assembly of the "necrosome" complex, in which Receptor Interacting Protein kinase 3 (RIP3) interacts with RIP1, Fas-Associated protein with Death Domain (FADD) and Caspase-8 upon a combined treatment of TNF-α, Smac-mimetic and pan-caspases inhibitors [27]. Unexpectedly, our latest data strongly suggested that the classical necrosome partners of RIP3 were not present in RIP3 containing complex in LN-18 glioma cells after 5-ALA-PDT treatment [21].

In the present study, we highlight the interference between a pro-necrotic RIP3 complex and a pro-survival TSC2-dependent pathway in glioblastoma treated by PDT.

2. Materials and methods

2.1. Cell culture

Human glioblastoma LN18, U87-MG and U373 cell lines were a kind gift of Pierre Robe (Human Genetics, GIGA-R, University of Liege, Belgium). F98 cells were kindly provided by Emmanuel Garçion (INSERM, Angers, France). T98G cell line was obtained from the ATCC. Cells were grown in DMEM complemented with 10% fetal bovine serum and 100 units mL^{-1} penicillin/streptomycin (Gibco) and maintained at 37 °C in a 5% CO_2 humidified atmosphere.

2.2. Plasmids single site directed mutagenesis and transfections

pcDNA3.0 3XHA-TSC2 (rat) WT (24939), and pcDNA3.0 FLAG-TSC2 (human) WT (14129) [28] plasmids were purchased *via* the Addgene they were deposited respectively by the Pr Kun-Liang Guan (University of California, San Diego) and Brendan D. Manning (Harvard T.H. School of Public Health). Control empty vector (EV) pcDNA3.0 3XHA was generated by digestion of the plasmid 24939, with *Not*I, *Xba*I and *Kpn*I restriction enzymes. pcDNA3.0 3XHA TSC2 (human) was constructed by cloning human TSC2 from the plasmid 14129 with the In-Fusion cloning system (Clontech). The Q5 High Fidelity DNA-Polymerase (NEB) was then used according the manufacturer to perform site directed mutagenesis to generate 3XHA-TSC2 (rat) S1254A and P1256A; and 3XHA-TSC2 (human) S1254A and P1256A mutants. For the establishment of stable cell lines, target cells were cultured until 80–90% of confluence in 6-well plates and transfected with 1 μg of the desired plasmid using the Lipofectamine LTX with Plus reagent (ThermoFisher Scientific) according to the manufacturer's instructions. 24 h later, cells were selected by a treatment with G-418 (1 $mg \cdot mL^{-1}$) (Roche).

2.3. Generation of TSC2 KO cells via the CRISPR system

Lentiviral plasmid targeting human TSC2 gene *via* CRISPR system was purchased from Sigma-Aldrich (pLenti U6gRNA TSC2-Cas9: Sigma-Aldrich HS0000020001 and HS0000019924) as well as the non-target guide (pLenti CRISPR-NT CONTROL: Sigma-Aldrich, CRISPR13-1EA). Guides will be referred lately as TSC2 #1, #2 and N.Targ, respectively. Briefly, Lenti-X 293T cells (Clontech) were co-transfected together with pLenti U6gRNA TSC2-Cas9 or pLenti CRISPR-NT CONTROL and pSPAX2-D64A (Addgene plasmid 12260 modified in order to mutate HIV-1 integrase catalytic site, non-integrative vector) or pSPAX2 (integrative vector) and a VSV-G encoding plasmids [29]. Lentiviral supernatants were collected 48 h, 72 h and 96 h post-transfection, filtrated and concentrated 100× by ultracentrifugation. The lentiviral vectors were then titrated with qPCR Lentivirus Titration (Titer) Kit (ABM, LV900) and used for cells transduction. After 72 h of transduction, cells expressing GFP were isolated by FACS. Each clone was allowed to grow and later tested by western blotting analysis and clones that were shown depleted for TSC2 were selected. For non-integrative clones a second FACS analysis was done after 2 weeks of culture in order to remove GFP expressing cells (rare event of integration of CAS9 DNA sequence). For integrative clones, cells were subjected to a regular puromycin treatment (5 $\mu g \cdot mL^{-1}$) (Invivogen).

2.4. Establishment of stables transduced cell lines

peGFP-RIP3 WT, RIP3 KD (D161N) (Kinase Dead) and RIP3 RHIM/AAAA (here after referred to as RHIMm) which were a kind gift from FK. Chan, were subjected to PCRs where 3XFLAG tag was added at the N-terminal part. 3XFLAG-RIP3-eGFPs amplicons were then cloned *via* the Gateway Cloning system (ThermoFisher Scientific) into a pLenti PGK Blast Dest plasmid (Addgene, 19065) [30] provided by the Dr. Eric Campeau (University of Massachusetts Medical School). LN-18 cells were infected and stable pools of cells expressing 3XFLAG-RIP3-eGFP selected with a blasticidin treatment (10 $\mu g \cdot mL^{-1}$) (Invivogen).

2.5. Purification of RIP3 immuno-complex

3XFLAG-RIP3-eGFP WT LN-18 transduced cells' proteins were extracted with a lysis buffer (20 mM Tris-HCl pH 7,4; 1% Triton X-100; 10% glycerol; 150 mM NaCl; 1 mM PMSF; 3.3 mM NaF, 1 mM Na3VO4, 25 mM glycerol-phosphate, Roche Complete™ protease inhibitor (Roche Life Science)). Incubated 20 min on ice, lysates were centrifuged at 15,000*g* for 15 min. The supernatant was collected and 56 mg of proteins was pre-cleared for 4 h at 4 °C with 100 μL of Protein-G beads (Santa Cruz Biotechnology, Dallas, TX), then incubated with 120 μL of FLAG-M2 beads (Sigma-Aldrich) overnight at 4 °C. Beads were then loaded on Poly-Prep Chromatography Columns (Bio-Rad) and washed with 50 mL of wash buffer (400 mM NaCl lysis buffer) and eluted with 4 mL of elution buffer (20 mM Tris-HCl pH 7,4; 150 mM NaCl; 200 $\mu g \cdot mL^{-1}$ of 3XFLAG peptide (Sigma-Aldrich)). The eluted proteins were concentrated on Vivaspin 500 columns (Sartorius) and resolved on a 4–12% SDS-PAGE (Invitrogen). The gel was finally analyzed with Sypro ruby staining (Invitrogen).

2.6. In-gel digestion and mass spectrometry (MS) analysis

In-gel digestion was performed by addition of modified trypsin (Promega, Madison, WI) in 50 mM ammonium bicarbonate at 37 °C overnight. The tryptic digests were air dried and then dissolved in formic acid (0.1%) for further MS-MS analysis. Each in-gel digest of an individual band was analyzed by nano-high-performance liquid chromatography (HPLC) electrospray MS-MS using an XCT ion trap mass spectrometer (Agilent, Santa Clara, CA). The HPLC separations were performed on an RP C18 Zorbax column from Agilent. The mobile phase was a 90 min gradient mixture formed as follows: mixture A, water-acetonitrile-formic acid (97/3/0.1 [v/v/v]); mixture B, acetonitrile-water-formic acid (90/10/0.1 [v/v/v]). The flow rate was fixed at 300 nL/min. The collision energy was set automatically depending on the mass of the parent ion. Each MS full scan was followed by MS-MS scans of the first four most intense peaks detected in the prior MS scan. A list of peptide masses was subsequently introduced into the database for protein identification searches using MASCOT (Matrix Sciences).

2.7. Reagents and antibodies

5-Aminolevulinic acid (5-ALA) and p38 inhibitor (S8307) was purchased from Sigma-Aldrich. MK2 inhibitor (MK2i, 475864) was bought from Merck Millipore. TNF-α was from Peprotech and zVAD-fmk was purchased from Promega. The BV6 Smac mimetic was previously described [21]. The following antibodies were used for western blot analysis: anti-FLAG-M2 (F-3165) and anti-RIP3 rat (R4277) (Sigma-Aldrich); anti-Caspase-8 (ALX-804-429) and anti-LC3 (NT-0231-100) (Enzo Life Sciences); anti-RIP1 (3493), anti-RIP3 human (13526), anti-TSC2

(4308), anti-Phospho-TSC2 rat (ser 1254) (3611), Phospho-4E-BP1 (Thr37/46) (236B4) and anti-Phospho-p38 MAPK (Thr180/Tyr182) (9211) (Cell Signalling Technology), anti-ATG7 (sc-12497), anti-YWHAE (sc-23957), anti-YWHAZ (sc-1019), anti-MK2 (sc-6221), anti-HA probe (sc-7392) (Santa Cruz Biotechnology); anti-Tuberin phospho S1254 human (ab133454) (Abcam); anti-GAPDH (AM4300) (Ambion).

2.8. PDT treatment

Cells were grown to 80% of confluence They were treated with 0.5 mM 5-ALA (Sigma) diluted in a free-phenol red complete growth medium for 3 h prior to irradiation with white light delivered by four fluorescent tubes (Aquarelle TLD-15W, Philips) with an irradiance of 23.70 $W \cdot m^{-2}$ and a light dose of 2.13 J cm^{-2}. Cells irradiation was performed in the free phenol red complete medium and was then collected and analyzed at the indicated time post-irradiation (pi).

2.9. RNAi transfection

A pool of four RNAi duplexes (smartpool) targeting human RIP3 (M-003534-01-0005), TSC2 (M-003029-03-0005), MK2 (M-003516-02-0005) and ATG7 (M-020112-01-0005) were purchased from Dharmacon. RNAi against human YWHAZ was designed with the BLOCK-iT™ RNAi Designer tools (Invitrogen) (5′-AGTTCTTGATCCCCAATGC-3′). Control RNAi was purchased from Applied Biosystems. RNAis were used at a concentration of 50 nM and transfection performed using calcium phosphate (ProFection® Mammalian Transfection System, Promega).

2.10. Confocal imaging and immunofluorescence

Cells were fixed with 4% (w/v) paraformaldehyde for 10 min at room temperature at the indicated times post-PDT. They were then permeabilized with 0.1% Triton X-100 PBS (Sigma-Aldrich) for 10 min at room temperature and saturated for 1 h in PBS supplemented with 4% of BSA. HA antibody was then incubated for overnight at 4 °C. Later, slides were rinsed with PBS and incubated with Alexa secondary antibody (Invitrogen) for 1 h at room temperature. Cells were then washed with PBS and stained with Hoechst33342 (Acros Organics) 1/50,000. After water rinsing, slides were mounted with mowiol. Samples were analyzed using a Leica TCS SP5 confocal microscope (Leica).

2.11. Western blot analysis

Western blots were performed on the indicated extract. Total lysates were obtained by resuspension of cells in total lysis buffer (50 mM Tris-HCl pH 7.5, 150 mM NaCl, 1% Na-deoxycholate, 1% NP-40, 1 mM PMSF, Roche complete protease inhibitor and Halt™ Phosphatase Inhibitor cocktail (ThermoFisher)). The western blot procedure has been previously published [31].

2.12. Co-immunoprecipitation experiments

Briefly, cells were lysed in the IP buffer (40 mM HEPES-HCl pH 7.4, 150 mM NaCl, 1% Triton X-100, 5% glycerol, 1 mM $MgCl_2$, 1 mM PMSF, Roche complete protease inhibitor and Halt™ Phosphatase Inhibitor cocktail (ThermoFisher)) and about 1 mg of protein was precleared at 4 °C for 1 h with A/G magnetic beads (ThermoFisher) while target or control antibody was incubated 1 h with the beads at room temperature. Cell lysates were then incubated with antibody coupled beads 4 h at 4 °C. Beads were then washed five times with the wash buffer (450 mM NaCl IP buffer). Immunoprecipitates were then eluted for 10 min on ice with a 2% sodium dodecylsulfate (SDS) solution supplemented by 2× loading buffer (10 mM Tris-HCl pH 6,8; 1% SDS; 25% glycerol; 0,1 mM β-mercaptoethanol; 0,03% bromophenol blue) and loaded onto SDS-PAGE.

2.13. Necrosis measurement

Lactate dehydrogenase (LDH) release essay was performed as described previously [21]. Briefly, LDH enzyme released by necroptosis was measurement of the LDH enzyme activity in the cell supernatant. Propidium iodide incorporation cell death assay was conducted according the manufacturer procedure (Sigma). To summarize, cells were trypsinized, washed with PBS then stained with a 40 $\mu g \cdot mL^{-1}$ of propidium iodide solution (Sigma) and finally analyzed by FACS.

2.14. Quantification, significance and statistical analysis

Western blots quantifications were done using the "ImageQuant LAS 4000" software (GE). Observations exposed represent at least three independent experiments. Data are presented as mean ± SEM and were analyzed with the GraphPad Prism software. Statistical significance was determined using the specified test. $p \leq 0.05$ was considered significant.

3. Results

3.1. TSC2 promotes survival in glioblastoma after a 5-ALA-PDT treatment

As previously mentioned, glioblastoma cells undergo cytoprotective autophagy following 5-ALA-PDT [14]. In the study of the upstream autophagy regulators potentially involved in this process, we found that siRNA-mediated silencing of TSC2 sensitized LN-18 glioblastoma cells to 5-ALA-PDT treatment (Fig. 1A). To validate our observation, we generated TSC2 knock out LN-18 cell lines using the CRISPR/Cas9 technology. The TSC2 knocked-out cells were more sensitive to induction of PDT mediated cell death, indicating that TSC2 might have a pro-survival role in these cells (Fig. 1B). We confirmed these findings by looking at additional glioma cell lines and we found that in the absence of TSC2, survival U87, T98G and U373 cells were significantly decreased following 5-ALA-PDT treatment (Fig. 1C). Altogether, these analyses strongly indicate that TSC2 might protect glioblastoma cells from 5-ALA-PDT-induced cell death.

3.2. TSC2 binds YWHAZ upon a phosphorylation of S1254 by MK2

While investigating the molecular mechanisms underlying the pro-survival function of TSC2 during PDT, we found that phosphorylation of TSC2 serine 1254 was induced by PDT treatment (Fig. 2A). Interestingly, this serine is known to potentially regulate the mTOR complex when being phosphorylated [32,33]. Closer examination revealed that phosphorylation of S1254 follows a biphasic kinetic: a first increase occurred as early as 15 min post-PDT. This level of S1254 phosphorylation is maintained up to 2 h post-treatment, at which it underwent a second increase and reached a maximum 4 h post-irradiation as presented by our quantification analysis (Fig. 2B). When looking at TSC2 amino-acid sequence, we found that S1254 lies within a canonical binding site for 14-3-3 proteins (R/KXXS/TXP) [32]. Therefore, we decided to investigate the formation of a TSC2/14-3-3 complex during PDT. Because high levels of YWHAZ (14-3-3 ξ) in glioblastoma tumors correlate with poor patient prognosis [34], we decided to focus our attention on this particular member of the 14-3-3 family. Co-immunoprecipitation analysis showed that TSC2 associated with YWHAZ following induction of PDT (Fig. 2A). In addition, PDT-induced TSC2/YWHAZ interaction was confirmed endogenously (Fig. 2C). Interestingly, association between TSC2 and YWHAZ correlates with elevated levels of S1254 phosphorylation. Co-immunoprecipitation experiments between wt and S1254 phosphorylation mutants of TSC2 revealed that interaction with YWHAZ relies on the presence of a phosphorylatable serine at position1254 (Fig. 2D). In agreement

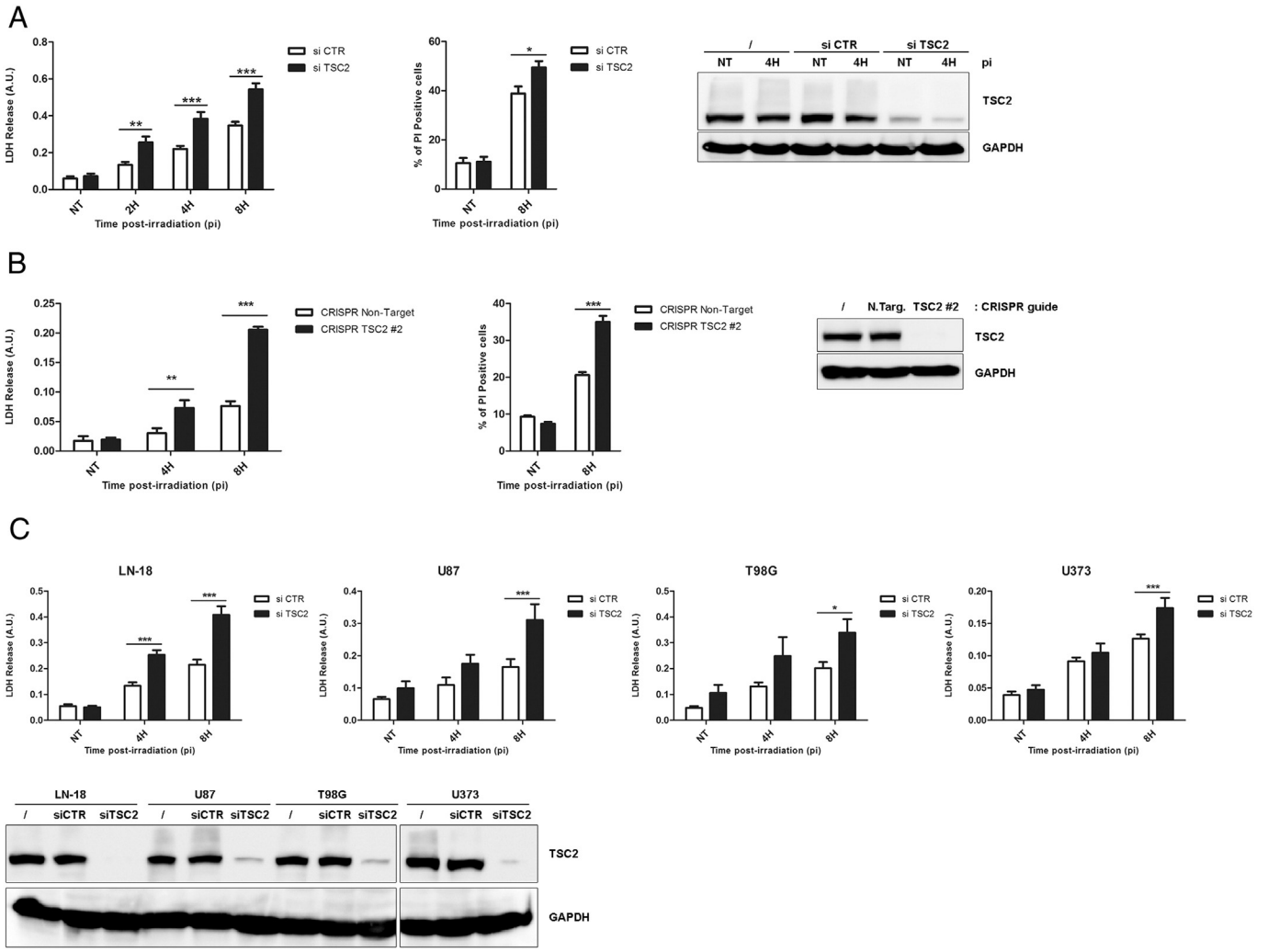

Fig. 1. TSC2 protects glioblastoma from 5-ALA-PDT-induced cell death. (A) LN-18 were transfected with smartpool targeting TSC2 was used to silence hTSC2 (n = 6). Cell death was measured by lactate dehydrogenase (LDH) release and propidium iodide incorporation assays compared to RNAi control (si CTR) at different time post-irradiation. Protein expression depletion was evaluated by western blotting analysis on total lysate of untransfected cells (/), RNAi control transfected cells and target protein RNAi transfected cells and were harvested at 4 h post-irradiation. GAPDH is a loading control. (B) LN-18 non-stably transduced by CRISPR cas9 guide Non Target (N.Targ.) or targeting TSC2 (TSC2 #2) were subjected to PDT and cell death was measured by the LDH release and propidium iodide incorporation assays at the indicated times post-irradiation (pi). TSC2 protein expression level was analyzed by western blotting. GAPDH was used as loading control (n = 3). (C) LN-18, U87, T98, and U373 glioma cells were transfected with RNAi control (si CTR) or TSC2 smartpool (si TSC2) and were subjected to PDT. Cell death was measured by LDH release assay at the indicated time post-irradiation. TSC2 protein expression level was analyzed by western blotting and GAPDH used as loading control (n = 3). (n = x, number of independent experiments; NT = untreated; pi = time post-irradiation; $^{*}p < 0.05$, $^{**}p < 0.01$, $^{***}p < 0.001$, *t*-test.)

with canonical 14-3-3-dependent sites, a proline is found at position +2 relative to S1254 (P1256). Interestingly, mutation of this proline into alanine abolished both interaction with YWHAZ and phosphorylation of Ser1254 (Fig. 2D). These observations suggest that association with YWHAZ might protect S1254 from dephosphorylation, as previously described for other 14-3-3 targets [35,36]. Supporting this, we found that preventing binding of YWHAZ by incubation of cell lysate with an R18 peptide, a well-described antagonist of 14-3-3s [37] decreases the level of S1254 phosphorylation (Fig. 2E).

MAPKAPK2 (MK2) has been reported to phosphorylate TSC2 on serine 1254 [38]. Accordingly, treatment with an MK2 inhibitor (MK2 Inhib, CAS 1186648-22-5) prevented PDT-induced TSC2 S1254 phosphorylation and interaction with YWHAZ (Fig. 2F). MK2 is a downstream kinase of p38 MAPK, known to be activated after PDT [39]. Therefore we studied p38 activation in our model. By looking at phosphorylation of Thr180/Tyr182 within p38 regulatory sites we found that p38 was activated 4 h post-treatment, suggesting that a p38/MK2 axis is activated after 5-ALA-PDT in glioblastomas (Fig. 2G).

3.3. Phosphorylation of TSC2 S1254 by MK2 constitutes a pro-survival axis after 5-ALA-PDT

To investigate the relevance of TSC2 S1254 phosphorylation during 5-ALA-PDT, we first knocked down expression of MK2 by RNAi (Fig. 3A) or inhibited its activity using a small molecule inhibitor (Fig. 3B). Both approaches significantly increased the sensitivity of LN-18 cells towards PDT treatment. In addition, inhibition of the MK2-activating kinase p38 also led to a reduction in LN-18 cell survival following PDT (Fig. 3C). The above observations suggested that phosphorylation of TSC2 by the p38/MK2 axis is important for TSC2 protective function during PDT. Since we showed that phosphorylation of S1254 promotes recruitment of YWHAZ, we decided to investigate the role of YWHAZ during PDT. Knocking down expression of YWHAZ by RNAi resulted in increased cell death after PDT, supporting the idea that phosphorylation of TSC2 S1254 and concomitant recruitment of YWHAZ are important for the protective function during PDT (Fig. 3D). To test this hypothesis, we expressed wt or S1254 phosphorylation mutants of TSC2 in the TSC2 KO LN-18 cells (Fig. 3E). As expected, expression

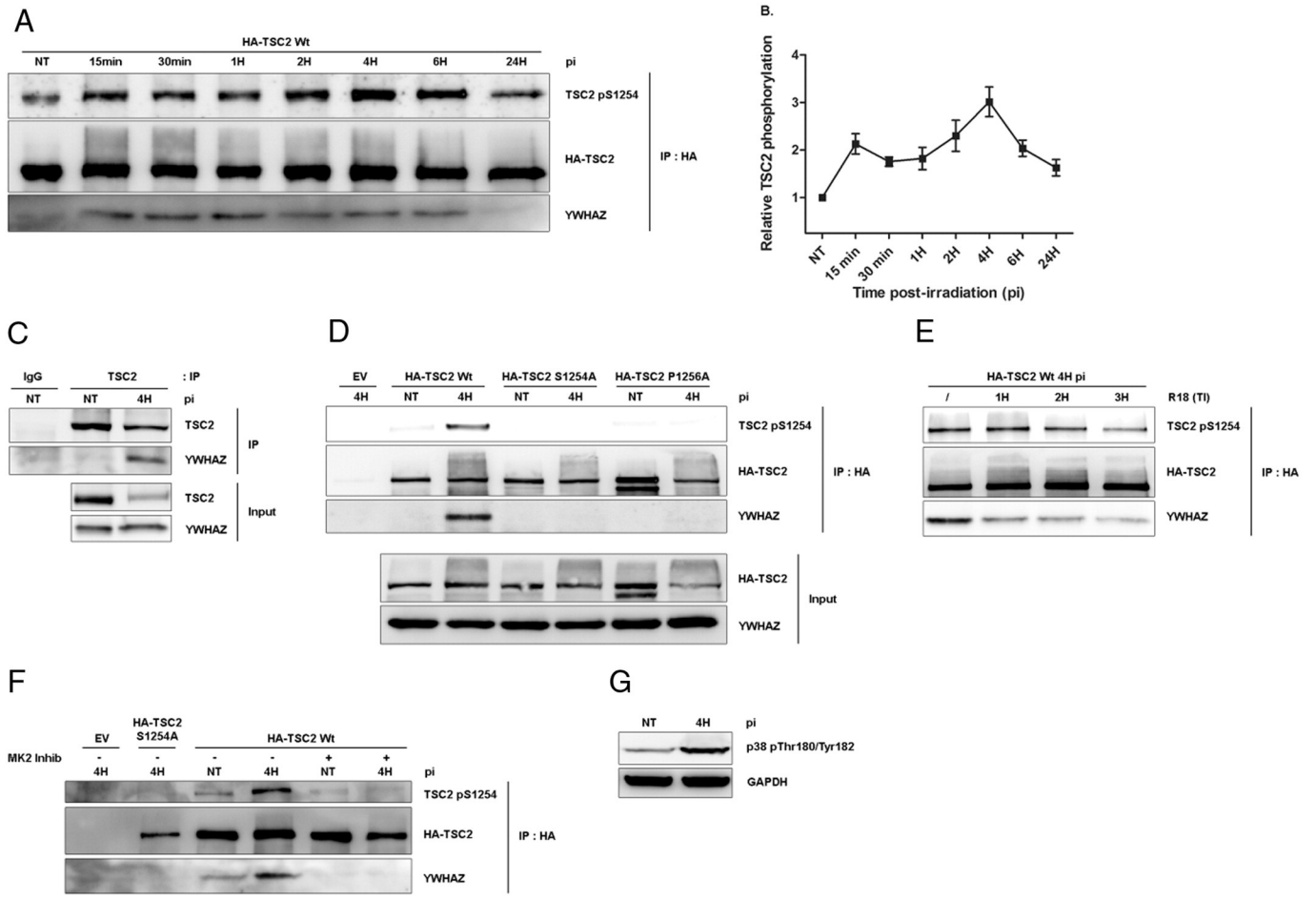

Fig. 2. TSC2 serine 1254 is phosphorylated by MK2 and binds YWHAZ after 5-ALA-PDT. (A) LN-18 cells were stably transfected with empty vector (EV) or by 3xHA-TSC2 (rat) wild type (wt). Cells were then treated by PDT and harvested at the indicated time post-irradiation and lysates subjected to an HA immunoprecipitation. Eluates were loaded on SDS-PAGE for western blotting analysis with TSC2 pS1254, HA or YWHAZ antibodies. (B) Relative quantification of TSC2 S1254A phosphorylation signal of the above experiment compared to untreated condition (n = 3). (C) LN-18 cells were treated by PDT and harvested at 4 h post-irradiation and lysates subjected to an TSC2 or control IgG immunoprecipitation. Eluates were loaded on SDS-PAGE for western blotting analysis with TSC2 and YWHAZ antibodies. (D) LN-18 cells were stably transfected with an empty vector (EV) or 3xHA-TSC2 (rat) wild type (wt), S1254A and P12565A and selected. Cells were then treated by PDT and lysates subjected to an HA immunoprecipitation. Eluates were loaded on SDS-PAGE for western blotting analysis with TSC2 pS1254, HA, or YWHAZ antibodies. (E) LN-18 cells were stably transfected by 3xHA-TSC2 (rat) wild type (wt). Cells were treated by PDT and lysates incubated with the R18 peptide (25 μM) for the indicated time (TI). Then, they were submitted to an HA immunoprecipitation and the eluate was loaded on SDS-PAGE for western blotting analysis with TSC2 pS1254, HA, YWHAZ antibodies. (F) LN-18 cells were stably transfected with empty vector (EV) or by 3xHA-TSC2 (rat) wild type (wt) or S1254A. Cells were then treated by PDT in presence of MK2 inhibitor (MK2 Inhib, 10 μM) and lysates subjected to an HA immunoprecipitation. Eluates were loaded on SDS-PAGE for western blotting analysis with TSC2 pS1254, HA, or YWHAZ antibodies. (G) LN-18 cells were harvested 4 h post-irradiation. Total lysates were analyzed by western blotting with a p38 pThr180/Tyr182 antibody, GAPDH was used as loading control. (IP = immunoprecipitation; pi = time post-irradiation; NT = non-treated.)

of hTSC2 wild type (wt) significantly restored LN-18 cell survival 4 and 8 h after PDT treatment. In contrast expression of hTSC2 S1254A or P1256A was unable to compensate for the absence of endogenous TSC2. Interestingly, expression of S1254 in the TSC2 null-background further promoted PDT-induced cell death. Altogether, these results demonstrate that TSC2 prevents PDT-induced cell death in glioblastoma cells, through a mechanism that relies on S1254 phosphorylation-mediated recruitment of YWHAZ.

Because we previously published that glioblastoma cells treated with 5-ALA-PDT activate a protective autophagic pathway [14], we tested the potential role of TSC2 in this process using our TSC2 mutants expressing cells lines. As expected, cells expressing wt hTSC2 increased by 5-fold their LC3-I-to LC3-II conversion after PDT treatment. In contrast, cells expressing hTSC2 S1254A and P1256A did not show any increase in autophagy fluxes (Fig. 3F). Interestingly, mTOR activity, as assessed by phosphorylation of its downstream target 4EB-P1 was dramatically increased in S1254 and P1256 mutant expressing cells, as compared to cells expressing wt TSC2 (Fig. 3F). Finally, RNAi knockdown of ATG7 which abolishes the basal and the induced macroautophagy, strongly increases the PDT-induced cell death in EV, hTSC2 Wt, S1254 and P1256A expressing cells. Intriguingly, a higher cell death induction was observed in EV, hTSC2 S1254 and P1256A compared to hTSC2 wt expressing cells. The latest suggesting that TSC2 serine 1254 phosphorylation might protect glioma from PDT through multiple mechanisms including autophagy. Altogether these data strongly support the idea that the ability of TSC2 to promote induction of autophagy and cell survival after 5-ALA-PDT relies on phosphorylation of its serine 1254 and recruitment of YWHAZ.

3.4. RIP3 forms a protein complex with RIP1, TSC2 and YWHAZ in glioblastoma after 5-ALA-PDT

As mentioned above, RIP3 is a key protein of the programmed necrosis pathway. RIP3 is activated and promotes cell death in glioblastoma after 5-ALA-PDT [21]. Therefore, we were interested to know if there was a crosstalk between the above described TSC2-dependent survival events and the RIP3-mediated cell death pathway. Moreover, YWHAZ and TSC2 have been found in two high throughput studies to potentially interact with RIP3 [40,41].

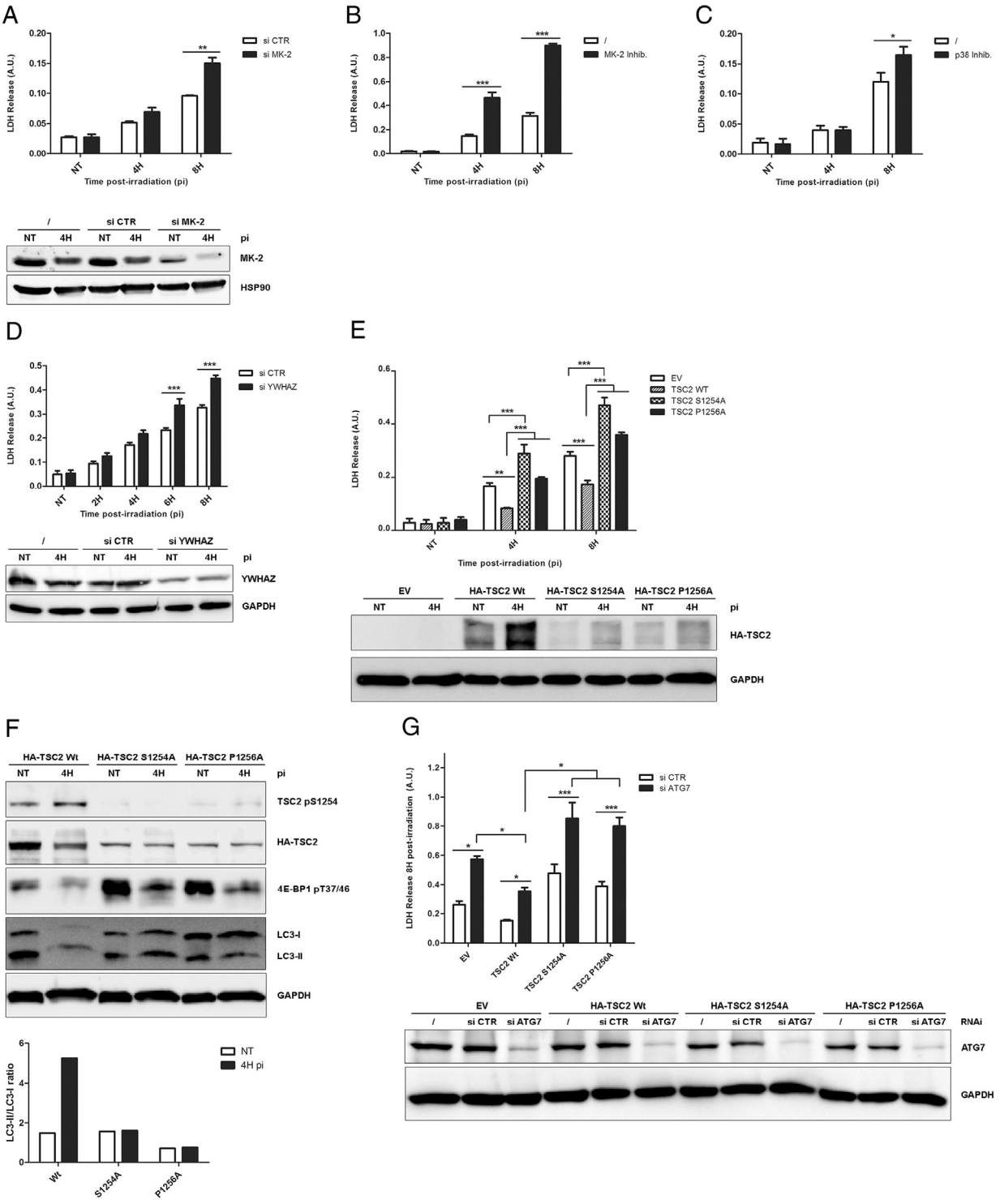

Fig. 3. Phosphorylation of TSC2 serine 1254 promotes survival through the activation of autophagy after 5-ALA-PDT. (A and D) LN-18 indicated proteins were silenced and cell death measured by lactate dehydrogenase (LDH) release assay compare to RNAi control (si CTR) at different time post-irradiation. Protein expression depletion was evaluated by a western blotting analysis on total lysate of untransfected cells (/), RNAi control transfected cells and target protein RNAi transfected cells and harvested at 4 h post-irradiation. GAPDH is a loading control. (A) LN-18 were transfected with a MK2 smart-pool targeting hMK2 (si MK2) and subjected to PDT (n = 3). MK2 protein expression level was analyzed by western blotting and HSP90 used as loading control. LN-18 cells were treated by MK2 (B) or p38 (C) inhibitors and cell death measured by LDH release assay at the indicated times post-irradiation (n = 3). (D) LN-18 were transfected with RNAi targeting YWHAZ to silence hYWHAZ (n = 3). Protein extinction was analyzed by western blotting, GAPDH is a loading control. (E) LN-18 were transduced and selected for 3xFlag-RIP3-eGFP wt. Cells were then transduced by CRISPR Cas9 TSC2 targeting non integrative vector (TSC2 #2). Cells were then stably transfected with an empty vector (EV) or by 3xHA-TSC2 (human) wild type (wt), S1254A and P12565A. Cells were then subjected to PDT and cell death was measured by LDH release assay at the indicated time post-irradiation (n = 3). HA-TSC2 proteins expression level was analyzed by western blotting with an HA antibody and GAPDH used as loading control. (F) LN-18 3xFlag-RIP3-eGFP, endogenous TSC2 knockout expressing 3xHA-TSC2 (human) wild type (wt), S1254A and P12565A (see above) were treated by PDT and harvested 4 h post-irradiation. Total lysates were loaded on SDS-PAGE and analyzed by western blotting with HA and the indicated antibodies (upper panel). Representative LC3-II/LC3-I ratio was quantified and analyzed (lower panel). (G) LN-18 3xFlag-RIP3-eGFP, endogenous TSC2 knockout expressing EV, 3xHA-TSC2 (human) wild type (wt), S1254A and P12565A (see above) were silenced for human ATG7 protein. Cell death was then measured by lactate dehydrogenase (LDH) release assay compare to si CTR 8 h post-irradiation. Protein expression depletion was evaluated by a western blotting analysis on total lysate of untransfected cells (/), RNAi control transfected cells and target protein RNAi transfected cells. GAPDH is a loading control (n = 4). (n = x, number of independent experiments; NT = non-treated; IP = immunoprecipitation; pi = time post-irradiation; $^{*}p < 0.05$, $^{**}p < 0.01$, $^{***}p < 0.001$, *t*-test.)

To tackle this hypothesis, we choose a totally different strategy. We first transduced LN-18 glioblastoma cell line with hRIP3 tagged with 3xFlag- at the N-terminus and eGFP at the C-terminus. Then, we checked if tagged-RIP3 was able to form the classic necroptotic complex with RIP1 and the caspase-8 upon a combined treatment of TNF-α, Smac-mimetic and z-VAD-fmk (TSzvD) [27]; and confirmed the formation of RIP3 clusters after 5-ALA-PDT and TSzvD treatments by confocal microscopy as showed previously [21,42] (Supplementary Fig. S1).

Secondly, we performed a proteomic analysis on the eluate of a 3xFlag-RIP3-eGFP immunoprecipitate harvested 4 h post-irradiation or in untreated condition (Fig. 4A). More than one hundred hits were found (Supplementary Table S1), and among them YWHAE, a 14-3-3 protein.

Based on our own observation that TSC2 interacts with 14-3-3 proteins, we investigated the potential interaction between RIP3, the 14-3-3s and TSC2. We first validated the new interactions of YWHAE, YWHAZ and TSC2 with RIP3 in our over-expression model by co-immunoprecipitation experiments at 4 h after treatment. RIP1 was used as RIP3 complex induction control (Fig. 4B). Surprisingly, RIP3 interacts stronger with TSC2 in treated conditions than in untreated cells whereas YWHAZ only interacts with RIP3 after PDT treatment. Interestingly, TSC2/RIP3 and RIP3/YWHAZ PDT-induced interactions were confirmed in a rat F98 glioblastoma cell line endogenous model (Fig. 4C). We next performed an immunofluorescence experiment and observed a diffused localization of RIP3 and TSC2 in untreated cells and a nucleation concomitant to a co-localization of both proteins 4 h after PDT (Fig. 4D). This observation supports the hypothesis of a TSC2/RIP3 complex formation after PDT. Unexpectedly, it is to notice that TSC2 total protein expression was perturbed by PDT as assessed by western blot analysis at different time point after PDT treatment. Actually, TSC2 protein level was significantly decreased starting from 2 h following PDT and returned to basal level 24 h after the treatment. To the contrary, RIP3 and YWHAZ protein levels were not affected (Supplementary Fig. S2). Finally as previously showed [21], we confirmed RIP3 implication in the glioblastoma cell death mechanism using RNAi where RIP3 silencing correlated with decreased PDT-induced cell death (Fig. 4E). Intriguingly, RIP3 is the only pro-death protein in the TSC2/YWHAZ/RIP3 complex, but it is to notice that TSC2 cell death sensitivity was not correlated to the expression level of RIP3 protein as shown by western blots analysis in different glioma cell lines (Supplementary Fig. S3).

3.5. TSC2/RIP3/14-3-3 complex stoichiometry is affected by RIP3 KD and RHIM mutations

RIP3 is a Serine/Threonine kinase and is able to form amyloid-like structure with its RHIM (RIP Homotypic Interacting Motif) domain, localized in its C-terminal part [42]. Therefore we checked the influence of KD (Kinase Dead) and RHIM (RIP Homotypic Interacting Motif) RIP3 mutations, respectively abrogating the kinase activity of RIP3 and its ability to multimerize with RIP1 after PDT, as previously described [31]. By TSC2 immunoprecipitation, we showed that RIP3-KD mutant was poorly recruited to TSC2 while the RHIM mutant interaction with TSC2 was enhanced compared to RIP3-wt. Inhibition of RIP1 kinase activity by necrostatin-1 does not interfere with the RIP3/TSC2 complex stoichiometry, demonstrating that RIP kinase 1 activity is not required for the formation of the RIP3 kinase containing complex (data not shown). YWHAZ was recruited to TSC2 after PDT treatment as well, with an interaction enhancement in the RIP3-RHIM condition (Fig. 4F). Intriguingly, YWHAZ immunoprecipitation showed its robust interaction with RIP3 wt after PDT and, respectively a decrease and an enhancement of its interactions with RIP3-KD and RIP3-RHIM (Fig. 4F). Together, these data suggest that TSC2 might interact with RIP3 through multiple interfaces.

3.6. RIP3/TSC2 interaction is modulated by TSC2 S1254 phosphorylation

As we identify S1254 of TSC2 as key of TSC2-mediated survival after PDT, we next asked whether RIP3 preferentially interacted with S1254 phosphorylated version of TSC2. Interestingly, TSC2 phosphorylated on serine 1254 strongly interacted with RIP3 (Fig. 5A). On top of that, the signal level of TSC2 phosphorylated on serine 1254 is similar in both RIP3 and TSC2 immunoprecipitates suggesting that the majority of TSC2 phosphorylated on S1254 interacts with RIP3 (Fig. 5A). To better understand the underlying mechanisms, we wondered whether phosphorylation of S1254 of TSC2 would be involved in the regulation of its interaction with RIP3. Then we first carried out co-immunoprecipitation experiments between rTSC2 wt, S1254A and P1256A mutants of TSC2 and RIP3. Interestingly, after PDT, interactions with RIP3 were significantly increased with both TSC2 mutants than with the wild type, suggesting that phosphorylation of S1254 might interfere with RIP3 binding (Fig. 5B and Fig. 5C). Supporting this, we found that promoting dephosphorylation of TSC2 S1254 by preventing YWHAZ binding with the R18 peptide increased the TSC2/RIP3 interaction, both in untreated and PDT-treated lysates (Fig. 5D). Finally, inhibition of the TSC2 S1254 MK2 kinase significantly enhances interaction between RIP3 and TSC2 after PDT (Fig. 5E and Fig. 5F). As expected, the recruitment of S1254 phosphorylated TSC2 on RIP3 is affected by MK2 inhibitor treatment as shown by quantification analysis of the ratio between S1254 phosphorylated TSC2 and total TSC2 recruited to RIP3 (Fig. 5G). This observation strengthens our hypothesis where RIP3 interacts with the whole available pool of S1254 phosphorylated form of TSC2. Altogether, these observations suggest that through recruitment of YWHAZ, phosphorylation of TSC2 S1254 by MK2 regulates the interaction between RIP3 and TSC2.

3.7. RIP3 binds stronger YWHAZ if TSC2 is inactive

YWHAZ is recruited to TSC2 under the phosphorylation of S1254 by MK2. Studying RIP3-immunocomplex in presence of MK2 kinase inhibitor after PDT, we were interested to know if YWHAZ/RIP3 interaction would be modulated by this small molecule. Interestingly, we found that as TSC2, YWHAZ is strongly recruited to RIP3 than in the control condition (Fig. 5E), suggesting that YWHAZ better interacts with RIP3 when TSC2 is not phosphorylated on serine 1254 and is not able to recruit YWHAZ, as demonstrated above. Finally, we wondered about the origin of YWHAZ interaction with RIP3. For this, we generated TSC2 KO LN-18 with the CRISPR/Cas 9 technology and transduced them with tagged-RIP3. Surprisingly, the absence of TSC2 does not affect the formation YWHAZ/RIP3 complex after PDT (Fig. 5H). These data suggest that RIP3 recruitment of YWHAZ is in competition with TSC2.

Altogether, we know that RIP3 is the only pro-death protein in the TSC2/YWHAZ/RIP3 complex and its interaction with TSC2 and YWHAZ seems to be precisely modulated by the critical pro-survival serine 1254 status. Moreover, our observations allowed us to propose that RIP3 antagonizes with the TSC2-dependent pro-survival pathway *via* dephosphorylation of TSC2 by competition for YWHAZ then the sequestration of TSC2 inactive forms.

4. Discussion

In this paper, using an unbiased proteomic approach, we have identified several new RIP3 partners involved in a pro-death complex and shown that this complex pro-death activity is counter-balanced by a TSC2/14-3-3s complex regulated *via* the p38 MAPK pathway. These results offer the first characterization of a regulated necrosis pathway induced in glioblastoma by an oxidative stress generated by PDT. This model is quite unique since the induction of necrosis in glioblastoma cells requires neither inhibition of capsase-8 activity nor the addition of Smac mimetics.

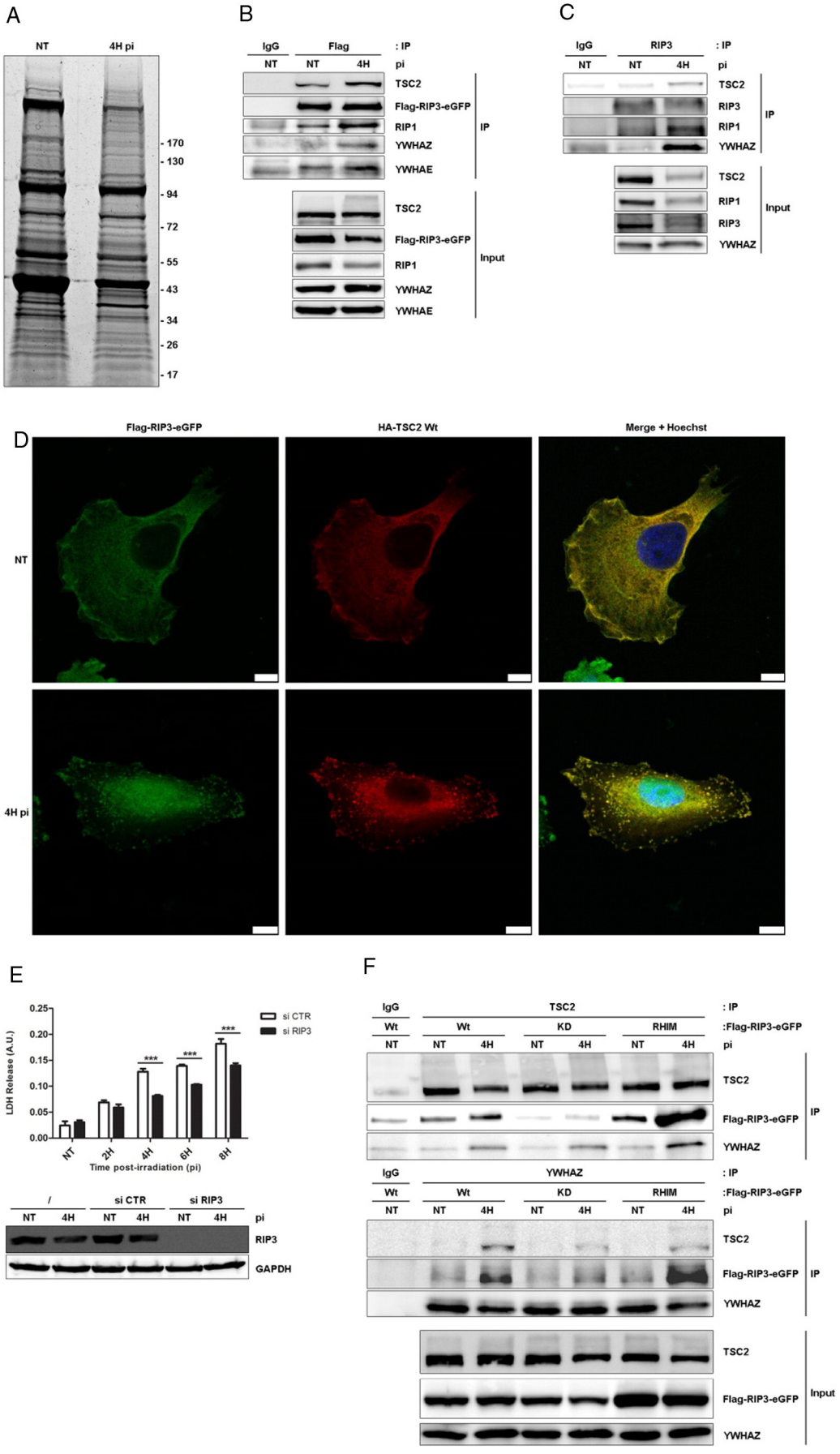
A
NT
4H pi
- 170
- 130
- 94
- 72
- 55
- 43
- 34
- 26
- 17
B
IgG
Flag
: IP
NT
NT
4H
pi
TSC2
Flag-RIP3-eGFP
RIP1
YWHAZ
YWHAE
IP
Input
C
IgG
RIP3
: IP
NT
NT
4H
pi
TSC2
RIP3
RIP1
YWHAZ
IP
Input
D
Flag-RIP3-eGFP
HA-TSC2 Wt
Merge + Hoechst
NT
4H pi
E
LDH Release (A.U.)
0.25
0.20
0.15
0.10
0.05
0.00
si CTR
si RIP3
***
***
***
NT
2H
4H
6H
8H
Time post-irradiation (pi)
/
si CTR
si RIP3
NT
4H
NT
4H
NT
4H
pi
RIP3
GAPDH
F
IgG
TSC2
: IP
Wt
Wt
KD
RHIM
:Flag-RIP3-eGFP
NT
NT
4H
NT
4H
NT
4H
pi
TSC2
Flag-RIP3-eGFP
YWHAZ
IP
IgG
YWHAZ
: IP
Wt
Wt
KD
RHIM
:Flag-RIP3-eGFP
NT
NT
4H
NT
4H
NT
4H
pi
TSC2
Flag-RIP3-eGFP
YWHAZ
IP
TSC2
Flag-RIP3-eGFP
YWHAZ
Input

PDT has been considered for a long time to induce apoptosis in different cell line models [20,43,44]. Therefore, our observation that PDT is able to induce necrosis in glioblastoma cells *in vitro* is quite unique and translates perfectly with *in vivo* observations showing important necrosis in treated tumors [23].

Since 2009, a canonical programmed necrosis pathway (necroptosis) has been described with RIP3 and RIP1 kinases as central key proteins. The signaling pathway triggered by TNF-α stimulation, requires Smac mimetic and pan-caspase inhibitors addition to induce a significant necroptotic cell death signal dependent on the formation of a RIP3/RIP1 complex [27]. Recently, other models of regulated necrosis involving or not RIP3 and RIP1 have been described: ferroptosis, NETosis or CYPD-dependent regulated necrosis [45]. Interestingly, our model of regulated cell death induced by 5-aminolevulinic acid-based PDT in LN-18 glioblastoma cells can be considered as a rare cellular model where necroptosis is triggered by a burst of ROS in mitochondria and *via* the activation of a RIP3-containing complex, but without any additional apoptosis inhibitors. In terms of activation, our glioblastoma model of necroptosis seems to be very relevant to what is observed *in vivo* following PDT but also following Ischemia/Reperfusion in the brain, heart and kidney [46].

Additionally, it is to notice that some groups described an autophagy-dependent cell death induced by PDT [47,48]. Autophagy is still considered as a key pathway for cancer treatment and especially with PDT, where it can lead primarily to a pro-survival pathway or in some circumstances to an autophagic cell-death induction [49,50]. In the case of glioblastoma, pro-autophagy drug treatments have been shown to significantly affect cell death [2] but this strategy cannot be applied to 5-ALA-PDT treatment of glioblastoma where the autophagy clearly protects glioblastoma and is suggested to eliminate PDT-damaged structures and proteins [14].

Our aforementioned experimental results reveal two main events appearing after 5-aminolevulinic acid-based PDT in glioblastoma cells. Firstly, from early time points after irradiation, we described the activation of a p38/MK2/TSC2/14-3-3 axis leading to the activation of a pro-survival autophagy. Secondly, at later time points, pro-death kinase RIP3 interacts with TSC2 and 14-3-3 proteins to down-regulate the above mentioned pro-survival action.

Role of p38 MAPK in cell survival after PDT-induced cell death is currently controversial [51]. In our study, p38 is related to an MK2-dependent phosphorylation of TSC2 serine 1254 which is suggested to be a clear pro-survival axis to activate a salutary autophagy which occurs as soon as 15 min after irradiation [14]. As we know that TSC2 activity is generally down-regulated in glioblastoma by upstream genetic alteration in the PI3K/AKT pathway [52], we were surprised to observe a pro-survival role of TSC2 after PDT. In addition, oppositely to PDT-treated cells, the basal level of glioblastoma cell death was not affected by the TSC2 or MK2 silencing indicating that these pro-survival-related events only occurred in stressed cells where the autophagy pathway is over-activated and mediates survival [14].

TSC2 S1254 phosphorylation pattern along the time post-irradiation is biphasic, which was unexpected. TSC2 is phosphorylated on serine 1254 from 15 min to 6 h after irradiation upon p38/MK2 axis activation with a peak 4 h post-treatment. At early stages, TSC2 activation seems to be a direct response to PDT-linked oxidative stress. However, TSC2 late phosphorylation appears concomitantly to RIP3-dependent cell death mechanisms activation as suggested by our RNAi study which showed that RIP3 affects cell death response only 4 h post-irradiation. This suggests that, at early time points after irradiation, TSC2-dependent survival pathway is not linked to the RIP3 cell death pathway by opposition to what is seen at later time points where the TSC2 phosphorylated form appears in a RIP3-containing complex mediating cell death activation.

Interestingly, our study precisely identified that MK2-dependent phosphorylation of TSC2 serine 1254 is a major event of the TSC2-dependent survival pathway. Moreover we showed that phosphorylation of this serine was directly linked to a pro-survival activation of autophagy. This rise of autophagic flux is suggested to be a consequence of a decreased mTOR activity when TSC2 serine 1254 is phosphorylated. It is to notice that only rare descriptions of TSC2 as a pro-survival factor have been described, and only in models where the autophagy was clearly identified as pro-survival [36].

From 15 min post-irradiation, we observed the formation of a complex where 14-3-3 proteins bound to TSC2 on an interaction site based on the phosphorylated serine 1254. In addition, we showed that 14-3-3s recruitment protects the S1254 phosphorylation against phosphatases and subsequently protects the pro-survival autophagy activation. Protective role of 14-3-3s was assessed by knock-down studies where their silencing enhances the cell sensitivity to PDT-induced cell death. This last observation was in accordance with previous studies in glioblastoma [34,53].

We know that RIP3 is the only pro-cell death protein in the TSC2/14-3-3 complex which formation has been assessed 4 h post-irradiation. Surprisingly, the whole pool of S1254 phosphorylated TSC2 seems to interact with RIP3. On the other hand, we described that TSC2 S1254 phosphorylation status is essential to activate the TSC2-dependent survival pathway, and seems to modulate TSC2/RIP3 complex stoichiometry. Concomitantly, we presented the recruitment of 14-3-3 proteins on TSC2 as a protective event against the dephosphorylation of the critical serine 1254. In addition, we showed that RIP3 binds strongly the 14-3-3s when TSC2 is not phosphorylated, suggesting that RIP3 competes with TSC2 for the binding of 14-3-3s.

So as a model, we propose that RIP3, by its competition mechanism, promotes a diminution of the TSC2-survival signal by decreasing the 14-3-3 proteins pool bound to TSC2 phosphorylated S1254 and so, inducing serine 1254 dephosphorylation. Finally, we suggest that non-phosphorylated TSC2 pool is trapped by RIP3 to avoid MK2 reactivation as shown by a stronger interaction of RIP3 with unphosphorylated form of TSC2. Our model is summarized in Fig. 6.

Interplays between necroptosis and autophagy pathways have been recently described. In particular, RIP3 has been identified to promote an autophagic response against coxsackievirus B3 infection in intestinal epithelial cells [54] or to directly interact with p62 [55] and Atg5 [56]. In our study, we suggest that RIP3 can interact and interfere with TSC2, another key player of the autophagic pathway.

Fig. 4. Formation of a TSC2/14-3-3/RIP3 protein complex after 5-ALA-PDT. (A) 56 mg of proteins was extracted with the IP buffer of 3xFlag-RIP3-eGFP LN-18 cells, harvested 4 h post-irradiation and the immunoprecipitation done as described in the Materials and methods section. (B) 3xFlag-RIP3-eGFP LN-18 transduced cells were treated by PDT and harvested 4 h post-irradiation. Lysates were then subjected to a Flag or control IgG immunoprecipitation. Eluates were loaded on SDS-PAGE for western blotting analysis with TSC2, Flag, RIP1, YWHAE or YWHAZ antibodies. (C) F98 cells were treated PDT and harvested 4 h post-irradiation. Lysates were then subjected to a RIP3 or control IgG immunoprecipitation. Eluates were loaded on SDS-PAGE for western blotting analysis with TSC2, RIP3, RIP1 or YWHAZ antibodies. (D) LN-18 3XFlag-RIP3-eGFP transduced cells were stably transfected with HA-TSC2 (human) wild type (wt), grown on coverslips and submitted to PDT treatment. Cells were then fixed, incubated with HA antibody. TSC2 and tagged-RIP3 localization was analyzed with a confocal microscope. Hoechst was used to identify the nucleus. (E) A smartpool targeting hRIP3 was used to silence RIP3 in LN-18 cells (n = 4). Cell death was measured by LDH release assay compare to RNAi control (si CTR) at different time post-irradiation. Protein expression depletion was evaluated by a western blotting analysis on total lysate of untransfected cells (/), RNAi control transfected cells and target protein RNAi transfected cells and harvested at the 4 h post-irradiation. GAPDH is used as loading control. (F) LN-18 were transduced by Flag-RIP3-eGFP wt, Kinase Dead mutant (KD) or RHIM mutant (RHIM) and harvested 4 h post-irradiation. Lysates were then subjected to a TSC2, YWHAZ or control IgG immunoprecipitation and eluates loaded on SDS-PAGE for western blotting analysis with TSC2, Flag, or YWHAZ antibodies. (NT = non-treated; IP = immunoprecipitation; pi = time post-irradiation; Input = total lysate extract; $^{***}p < 0.001$, *t*-test.)

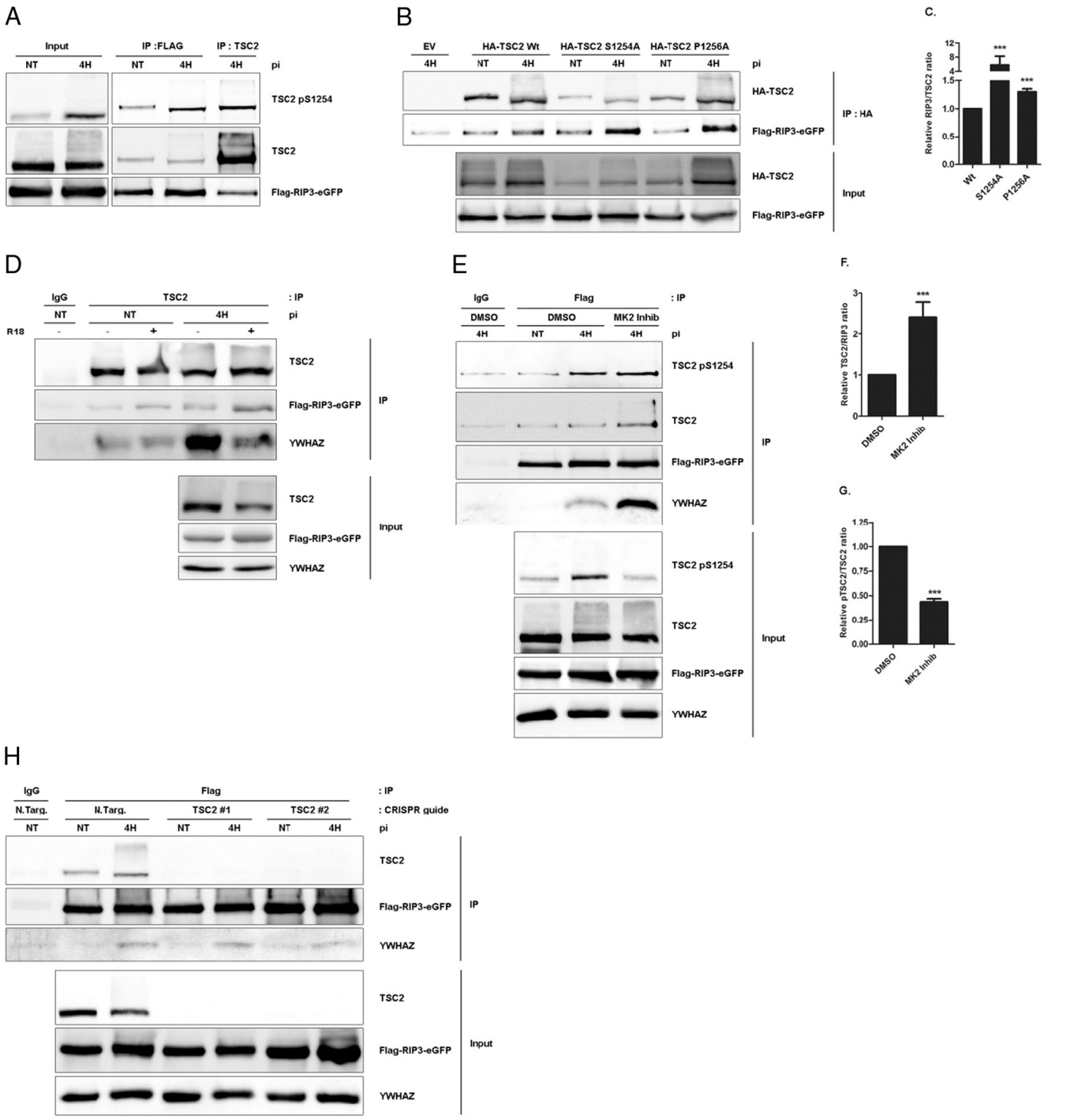

Fig. 5. TSC2 S1254 phosphorylation modulates the RIP3/TSC2 interaction after PDT. (A) LN-18 cells transduced by 3xFlag-RIP3-eGFP were treated by PDT and lysates subjected to a Flag or TSC2 immunoprecipitation. Eluates were then loaded on SDS-PAGE for western blotting analysis with TSC2 pS1254, TSC2 and Flag antibodies. (B) LN-18 cells were transduced by 3xFlag-RIP3-eGFP and stably transfected with an empty vector (EV) or by 3xHA-TSC2 (rat) wild type (wt), S1254A and P12565A. Cells were then treated by PDT and lysates subjected to an HA immunoprecipitation. Eluates were loaded on SDS-PAGE for western blotting analysis with HA and Flag antibodies. (C) Quantification and analysis of the RIP3/TSC2 ratio of the above HA immunoprecipitation (n = 3). (D) LN-18 cells transduced by 3xFlag-RIP3-eGFP were treated by PDT and lysates incubated with R18 peptide (25 μM) during TSC2 immunoprecipation. IgG immunoprecipitation was used as control. Eluates were then loaded on SDS-PAGE for western blotting analysis with TSC2, Flag and YWHAZ antibodies. (E) LN-18 cells transduced by 3xFlag-RIP3-eGFP were treated by PDT in the presence of MK2 inhibitor (MK2 Inhib, 10 μM) and lysates subjected to control IgG or Flag immunoprecipitation. Eluates were then loaded on SDS-PAGE for western blotting analysis with TSC2 pS1254, TSC2, Flag and YWHAZ antibodies. (F) Quantification and analysis of the TSC2/RIP3 ratio of the above Flag immunoprecipitation (n = 3). (G) Quantification and analysis of the ratio pTSC2/TSC2 immunoprecipitated with RIP3 (n = 3). (H) LN-18 was transduced by 3xFlag-RIP3-eGFP wt and by CRISPR Cas9 integrative vectors: Non Target (N.Targ.), TSC2 #1 and #2. Cells were then treated by PDT and lysates subjected to a Flag or control IgG immunoprecipitation. Eluates were loaded on SDS-PAGE for western blotting analysis with TSC2, Flag or YWHAZ antibodies. (n = x, number of independent experiments; NT = non-treated; IP = immunoprecipitation; pi = time post-irradiation; $^{***}p < 0.001$, *t*-test.)

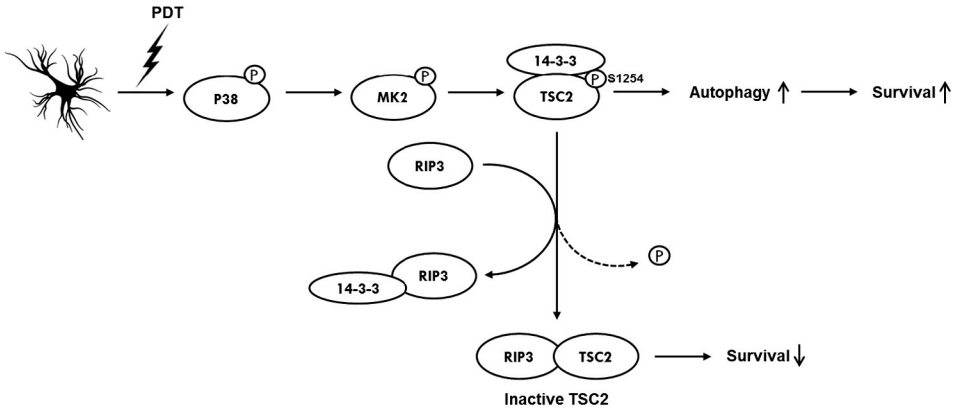

Fig. 6. Proposed survival mechanisms occurring in glioblastoma after 5-ALA-PDT. After PDT, p38 is phosphorylated and activated together with its downstream kinase MK2. MK2 then phosphorylates TSC2 on serine 1254 which recruits protective 14-3-3 proteins and promotes cell survival by the activation of the autophagy process. About 4 h post-treatment, cell death inducer RIP3 is activated and interacts with S1254 phosphorylated TSC2 protein pool. By a competition mechanism for the TSC2 linked 14-3-3 proteins, RIP3 mediates dephosphorylation of TSC2, traps the inactive TSC2 and thus down-regulates TSC2-dependent survival.

Interestingly, preliminary data showed that RIP3 also interacts with p62 after PDT. This interaction is reinforced when cells are treated with MK2 inhibitor (data not shown). These observations suggest that RIP3 would potentially target several proteins in the autophagic pathway, strengthening the idea that our cellular PDT system is potentially interesting to study cross-talks between RIP3 and the autophagy pathway.

From a clinical point of view, glioblastomas are currently still almost incurable. Current strategies only extend the patient lifetime but without possibility to eradicate the tumors. We definitively need fundamental research to discover new therapeutic approaches, novel ideas and new pathways to target for the patient's benefits. Moreover, it is obvious that therapeutic strategies even in the PDT field have to be customized to the tumor specificity of each patient. In the present study, we highlighted that pro-survival autophagy and the 14-3-3 proteins family are strong potential targets to enhance glioblastoma sensitivity to anti-tumors therapies. Moreover we clearly described MK2 and TSC2 as new potentials therapeutic targets in glioblastoma treatment by 5-ALA-PDT.

In conclusion, we described a new TSC2-dependent survival pathway which is triggered in glioblastoma in response to 5-aminolevulinic acid-based PDT. Moreover, this pathway seems to be targeted by RIP3, which binds TSC2 after PDT in order to fully induce necroptosis.

Contributions

GF designed and performed experiments, analyzed data and wrote the manuscript. CL performed experiments. LL, ED, FD, MF, IC and JP contributed to the design and interpretation of experiments and critically revised the manuscript. All the authors approved the final manuscript.

Competing interests

The authors declare no competing financial interests.

Transparency document

The Transparency document associated with this article can be found, in the online version.

Acknowledgments

We thank F. Giroulle and A. Cipolla from the GIGA-Viral Vector plateform (Liège, Belgium) for the generation of transduced cell lines. We thank R. Stephan and S. Ormenese from the GIGA-Imaging and flow cytometry platform (Liège, Belgium) for their help. We thank G. Cobraiville for the help during the proteomic analysis.

This research was funded by the Télévie (F.R.S. - FNRS, Brussels, Belgium; FC 92390) and the Centre Anti-Cancéreux fund (University of Liège, Belgium; 216589), the Belgian "Fonds National pour la Recherche Scientifique" (F.R.S. - FNRS; FRSM- 3.4537.11) and the Interuniversity Attraction Poles (IAP) program initiated by the Belgian Science Policy Office (BELSPO; P7/32).

Appendix A. Supplementary data

Supplementary data to this article can be found online at http://dx.doi.org/10.1016/j.bbamcr.2016.10.014.

References

[1] A. Omuro, L.M. DeAngelis, Glioblastoma and other malignant gliomas: a clinical review, JAMA 310 (2013) 1842–1850.
[2] R. Stupp, M.E. Hegi, W.P. Mason, M.J. van den Bent, M.J. Taphoorn, R.C. Janzer, S.K. Ludwin, A. Allgeier, B. Fisher, K. Belanger, P. Hau, A.A. Brandes, J. Gijtenbeek, C. Marosi, C.J. Vecht, K. Mokhtari, P. Wesseling, S. Villa, E. Eisenhauer, T. Gorlia, M. Weller, D. Lacombe, J.G. Cairncross, R.O. Mirimanoff, R. European Organisation for, T. Treatment of Cancer Brain, G. Radiation Oncology, G. National Cancer Institute of Canada Clinical Trials, Effects of radiotherapy with concomitant and adjuvant temozolomide versus radiotherapy alone on survival in glioblastoma in a randomised phase III study: 5-year analysis of the EORTC-NCIC trial, Lancet. Oncol. 10 (2009) 459–466.
[3] D.N. Louis, H. Ohgaki, O.D. Wiestler, W.K. Cavenee, P.C. Burger, A. Jouvet, B.W. Scheithauer, P. Kleihues, The 2007 WHO classification of tumours of the central nervous system, Acta Neuropathol. 114 (2007) 97–109.
[4] M. Weller, M. van den Bent, K. Hopkins, J.C. Tonn, R. Stupp, A. Falini, E. Cohen-Jonathan-Moyal, D. Frappaz, R. Henriksson, C. Balana, O. Chinot, Z. Ram, G. Reifenberger, R. Soffietti, W. Wick, G. European Association for Neuro-Oncology Task Force on Malignant, EANO guideline for the diagnosis and treatment of anaplastic gliomas and glioblastoma, Lancet. Oncol. 15 (2014) e395–e403.
[5] O.O. Kanu, B. Hughes, C. Di, N. Lin, J. Fu, D.D. Bigner, H. Yan, C. Adamson, Glioblastoma multiforme oncogenomics and signaling pathways, Clinical Medicine. Oncology 3 (2009) 39–52.
[6] M. Bredel, D.M. Scholtens, A.K. Yadav, A.A. Alvarez, J.J. Renfrow, J.P. Chandler, I.L. Yu, M.S. Carro, F. Dai, M.J. Tagge, R. Ferrarese, C. Bredel, H.S. Phillips, P.J. Lukac, P.A. Robe, A. Weyerbrock, H. Vogel, S. Dubner, B. Mobley, X. He, A.C. Scheck, B.I. Sikic, K.D. Aldape, A. Chakravarti, G.R.t. Harsh, NFKBIA deletion in glioblastomas, N. Engl. J. Med. 364 (2011) 627–637.
[7] B.J. Quirk, G. Brandal, S. Donlon, J.C. Vera, T.S. Mang, A.B. Foy, S.M. Lew, A.W. Girotti, S. Jogal, P.S. LaViolette, J.M. Connelly, H.T. Whelan, Photodynamic therapy (PDT) for malignant brain tumors—where do we stand? Photodiagn. Photodyn. Ther. 12 (2015) 530–544.
[8] I. Albert, M. Hefti, V. Luginbuehl, Physiological oxygen concentration alters glioma cell malignancy and responsiveness to photodynamic therapy in vitro, Neurol. Res. 36 (2014) 1001–1010.
[9] M. Ishizuka, F. Abe, Y. Sano, K. Takahashi, K. Inoue, M. Nakajima, T. Kohda, N. Komatsu, S. Ogura, T. Tanaka, Novel development of 5-aminolevurinic acid (ALA) in cancer diagnoses and therapy, Int. Immunopharmacol. 11 (2011) 358–365.

[10] W. Stummer, U. Pichlmeier, T. Meinel, O.D. Wiestler, F. Zanella, H.J. Reulen, Fluorescence-guided surgery with 5-aminolevulinic acid for resection of malignant glioma: a randomised controlled multicentre phase III trial, Lancet. Oncol. 7 (2006) 392–401.
[11] M.S. Eljamel, C. Goodman, H. Moseley, ALA and Photofrin fluorescence-guided resection and repetitive PDT in glioblastoma multiforme: a single centre Phase III randomised controlled trial, Lasers Med. Sci. 23 (2008) 361–367.
[12] S.S. Stylli, A.H. Kaye, L. MacGregor, M. Howes, P. Rajendra, Photodynamic therapy of high grade glioma - long term survival, Off. J. Clin. Neurosci.: J. Neurosur. Soc. Australas. 12 (2005) 389–398.
[13] W. Stummer, T. Beck, W. Beyer, J.H. Mehrkens, A. Obermeier, N. Etminan, H. Stepp, J.C. Tonn, R. Baumgartner, J. Herms, F.W. Kreth, Long-sustaining response in a patient with non-resectable, distant recurrence of glioblastoma multiforme treated by interstitial photodynamic therapy using 5-ALA: case report, J. Neuro-Oncol. 87 (2008) 103–109.
[14] I. Coupienne, S. Bontems, M. Dewaele, N. Rubio, Y. Habraken, S. Fulda, P. Agostinis, J. Piette, NF-kappaB inhibition improves the sensitivity of human glioblastoma cells to 5-aminolevulinic acid-based photodynamic therapy, Biochem. Pharmacol. 81 (5) (2010) 606–616.
[15] J. Huang, B.D. Manning, The TSC1-TSC2 complex: a molecular switchboard controlling cell growth, Biochem. J. 412 (2008) 179–190.
[16] C.F. Bento, A. Ashkenazi, M. Jimenez-Sanchez, D.C. Rubinsztein, The Parkinson's disease-associated genes ATP13A2 and SYT11 regulate autophagy via a common pathway, Nat. Commun. 7 (2016) 11803.
[17] A. Garcia-Aguilar, C. Guillen, M. Nellist, A. Bartolome, M. Benito, TSC2 N-terminal lysine acetylation status affects to its stability modulating mTORC1 signaling and autophagy, Biochim. Biophys. Acta 1863 (2016) 2658–2667.
[18] D.A. Guertin, D.M. Sabatini, Defining the role of mTOR in cancer, Cancer Cell 12 (2007) 9–22.
[19] Y. Miki, J. Akimoto, S. Yokoyama, T. Homma, M. Tsutsumi, J. Haraoka, K. Hirano, M. Beppu, Photodynamic therapy in combination with talaporfin sodium induces mitochondrial apoptotic cell death accompanied with necrosis in glioma cells, Biol. Pharm. Bull. 36 (2013) 215–221.
[20] M. Chakrabarti, N.L. Banik, S.K. Ray, Photofrin based photodynamic therapy and miR-99a transfection inhibited FGFR3 and PI3K/Akt signaling mechanisms to control growth of human glioblastoma in vitro and in vivo, PLoS One 8 (2013), e55652.
[21] I. Coupienne, G. Fettweis, N. Rubio, P. Agostinis, J. Piette, 5-ALA-PDT induces RIP3-dependent necrosis in glioblastoma, Photochem. Photobiol. Sci. 10 (2011) 1868–1878.
[22] Y. Miki, J. Akimoto, K. Moritake, C. Hironaka, Y. Fujiwara, Photodynamic therapy using talaporfin sodium induces concentration-dependent programmed necroptosis in human glioblastoma T98G cells, Lasers Med. Sci. 30 (2015) 1739–1745.
[23] M.C. Tetard, M. Vermandel, H.A. Leroy, B. Leroux, C.A. Maurage, J.P. Lejeune, S. Mordon, N. Reyns, Interstitial 5-ALA photodynamic therapy and glioblastoma: preclinical model development and preliminary results, Photodiagn. Photodyn. Ther. 13 (2016) 218–224.
[24] A. Das, D.G. McDonald, Y.N. Dixon-Mah, D.J. Jacqmin, V.N. Samant, W.A. Vandergrift 3rd, S.M. Lindhorst, D. Cachia, A.K. Varma, K.N. Vanek, N.L. Banik, J.M. Jenrette 3rd, J.J. Raizer, P. Giglio, S.J. Patel, RIP1 and RIP3 complex regulates radiation-induced programmed necrosis in glioblastoma, Tumour Biol.: J. Int. Soc. Oncodev. Biol. Med. (2015).
[25] L. Zhang, H. Wang, K. Ding, J. Xu, FTY720 induces autophagy-related apoptosis and necroptosis in human glioblastoma cells, Toxicol. Lett. 236 (2015) 43–59.
[26] S. Melo-Lima, M. Celeste Lopes, F. Mollinedo, Necroptosis is associated with low procaspase-8 and active RIPK1 and -3 in human glioma cells, Oncoscience 1 (2014) 649–664.
[27] S. He, L. Wang, L. Miao, T. Wang, F. Du, L. Zhao, X. Wang, Receptor interacting protein kinase-3 determines cellular necrotic response to TNF-alpha, Cell 137 (2009) 1100–1111.
[28] B.D. Manning, A.R. Tee, M.N. Logsdon, J. Blenis, L.C. Cantley, Identification of the tuberous sclerosis complex-2 tumor suppressor gene product tuberin as a target of the phosphoinositide 3-kinase/akt pathway, Mol. Cell 10 (2002) 151–162.
[29] N. Emi, T. Friedmann, J.K. Yee, Pseudotype formation of murine leukemia virus with the G protein of vesicular stomatitis virus, J. Virol. 65 (1991) 1202–1207.
[30] E. Campeau, V.E. Ruhl, F. Rodier, C.L. Smith, B.L. Rahmberg, J.O. Fuss, J. Campisi, P. Yaswen, P.K. Cooper, P.D. Kaufman, A versatile viral system for expression and depletion of proteins in mammalian cells, PLoS One 4 (2009), e6529.
[31] I. Coupienne, G. Fettweis, J. Piette, RIP3 expression induces a death profile change in U2OS osteosarcoma cells after 5-ALA-PDT, Lasers Surg. Med. 43 (2011) 557–564.
[32] S.D. Shumway, Y. Li, Y. Xiong, 14-3-3beta binds to and negatively regulates the tuberous sclerosis complex 2 (TSC2) tumor suppressor gene product, tuberin, J. Biol. Chem. 278 (2003) 2089–2092.
[33] Y. Li, K. Inoki, R. Yeung, K.L. Guan, Regulation of TSC2 by 14-3-3 binding, J. Biol. Chem. 277 (2002) 44593–44596.
[34] X. Yang, W. Cao, J. Zhou, W. Zhang, X. Zhang, W. Lin, Z. Fei, H. Lin, B. Wang, 14-3-3zeta positive expression is associated with a poor prognosis in patients with glioblastoma, Neurosurgery 68 (2011) 932–938 (discussion 938).
[35] M. Martin, M. Potente, V. Janssens, D. Vertommen, J.C. Twizere, M.H. Rider, J. Goris, S. Dimmeler, R. Kettmann, F. Dequiedt, Protein phosphatase 2A controls the activity of histone deacetylase 7 during T cell apoptosis and angiogenesis, Proc. Natl. Acad. Sci. U. S. A. 105 (2008) 4727–4732.
[36] L.K. Nutt, M.R. Buchakjian, E. Gan, R. Darbandi, S.Y. Yoon, J.Q. Wu, Y.J. Miyamoto, J.A. Gibbons, J.L. Andersen, C.D. Freel, W. Tang, C. He, M. Kurokawa, Y. Wang, S.S. Margolis, R.A. Fissore, S. Kornbluth, Metabolic control of oocyte apoptosis mediated by 14-3-3zeta-regulated dephosphorylation of caspase-2, Dev. Cell 16 (2009) 856–866.
[37] B. Wang, H. Yang, Y.C. Liu, T. Jelinek, L. Zhang, E. Ruoslahti, H. Fu, Isolation of high-affinity peptide antagonists of 14-3-3 proteins by phage display, Biochemistry 38 (1999) 12499–12504.
[38] Y. Li, K. Inoki, P. Vacratsis, K.L. Guan, The p38 and MK2 kinase cascade phosphorylates tuberin, the tuberous sclerosis 2 gene product, and enhances its interaction with 14-3-3, J. Biol. Chem. 278 (2003) 13663–13671.
[39] L.O. Klotz, C. Fritsch, K. Briviba, N. Tsacmacidis, F. Schliess, H. Sies, Activation of JNK and p38 but not ERK MAP kinases in human skin cells by 5-aminolevulinate-photodynamic therapy, Cancer Res. 58 (1998) 4297–4300.
[40] D.W. Zhang, J. Shao, J. Lin, N. Zhang, B.J. Lu, S.C. Lin, M.Q. Dong, J. Han, RIP3, an energy metabolism regulator that switches TNF-induced cell death from apoptosis to necrosis, Science 325 (2009) 332–336.
[41] X. Wu, L. Tian, J. Li, Y. Zhang, V. Han, Y. Li, X. Xu, H. Li, X. Chen, J. Chen, W. Jin, Y. Xie, J. Han, C.Q. Zhong, Investigation of receptor interacting protein (RIP3)-dependent protein phosphorylation by quantitative phosphoproteomics, Mol. Cell. Proteomics 11 (2012) 1640–1651.
[42] J. Li, T. McQuade, A.B. Siemer, J. Napetschnig, K. Moriwaki, Y.S. Hsiao, E. Damko, D. Moquin, T. Walz, A. McDermott, F.K. Chan, H. Wu, The RIP1/RIP3 necrosome forms a functional amyloid signaling complex required for programmed necrosis, Cell 150 (2012) 339–350.
[43] H. Inoue, Y. Kajimoto, M.A. Shibata, N. Miyoshi, N. Ogawa, S. Miyatake, Y. Otsuki, T. Kuroiwa, Massive apoptotic cell death of human glioma cells via a mitochondrial pathway following 5-aminolevulinic acid-mediated photodynamic therapy, J. Neuro-Oncol. 83 (2007) 223–231.
[44] S. Karmakar, N.L. Banik, S.J. Patel, S.K. Ray, 5-Aminolevulinic acid-based photodynamic therapy suppressed survival factors and activated proteases for apoptosis in human glioblastoma U87MG cells, Neurosci. Lett. 415 (2007) 242–247.
[45] T. Vanden Berghe, A. Linkermann, S. Jouan-Lanhouet, H. Walczak, P. Vandenabeele, Regulated necrosis: the expanding network of non-apoptotic cell death pathways, Nat. Rev. Mol. Cell Biol. 15 (2014) 135–147.
[46] S. Jouan-Lanhouet, F. Riquet, L. Duprez, T. Vanden Berghe, N. Takahashi, P. Vandenabeele, Necroptosis, in vivo detection in experimental disease models, Semin. Cell Dev. Biol. 35 (2014) 2–13.
[47] L.Y. Xue, S.M. Chiu, N.L. Oleinick, Atg7 deficiency increases resistance of MCF-7 human breast cancer cells to photodynamic therapy, Autophagy 6 (2010) 248–255.
[48] D. Kessel, A.S. Arroyo, Apoptotic and autophagic responses to Bcl-2 inhibition and photodamage, Photochem. Photobiol. Sci. 6 (2007) 1290–1295.
[49] A.D. Garg, H. Maes, E. Romano, P. Agostinis, Autophagy, a major adaptation pathway shaping cancer cell death and anticancer immunity responses following photodynamic therapy, Photochem. Photobiol. Sci. 14 (2015) 1410–1424.
[50] M. Dewaele, W. Martinet, N. Rubio, T. Verfaillie, P.A. de Witte, J. Piette, P. Agostinis, Autophagy pathways activated in response to PDT contribute to cell resistance against ROS damage, J. Cell. Mol. Med. 15 (6) (2010) 1402–1414.
[51] M. Broekgaarden, R. Weijer, T.M. van Gulik, M.R. Hamblin, M. Heger, Tumor cell survival pathways activated by photodynamic therapy: a molecular basis for pharmacological inhibition strategies, Cancer Metastasis Rev. 34 (2015) 643–690.
[52] S. Tanaka, D.N. Louis, W.T. Curry, T.T. Batchelor, J. Dietrich, Diagnostic and therapeutic avenues for glioblastoma: no longer a dead end? Nat. Rev. Clin. Oncol. 10 (2013) 14–26.
[53] A. Matta, K.W. Siu, R. Ralhan, 14-3-3 zeta as novel molecular target for cancer therapy, Expert Opin. Ther. Targets 16 (2012) 515–523.
[54] K.G. Harris, S.A. Morosky, C.G. Drummond, M. Patel, C. Kim, D.B. Stolz, J.M. Bergelson, S. Cherry, C.B. Coyne, RIP3 regulates autophagy and promotes coxsackievirus B3 infection of intestinal epithelial cells, Cell Host Microbe 18 (2015) 221–232.
[55] Y. Matsuzawa, S. Oshima, Y. Nibe, M. Kobayashi, C. Maeyashiki, Y. Nemoto, T. Nagaishi, R. Okamoto, K. Tsuchiya, T. Nakamura, M. Watanabe, RIPK3 regulates p62-LC3 complex formation via the caspase-8-dependent cleavage of p62, Biochem. Biophys. Res. Commun. 456 (2015) 298–304.
[56] F. Basit, S. Cristofanon, S. Fulda, Obatoclax (GX15-070) triggers necroptosis by promoting the assembly of the necrosome on autophagosomal membranes, Cell Death Differ. 20 (2013) 1161–1173.